Author Manuscript

Author Manuscript

Author Manuscript

Author Manuscript

HHS Public Access

Author manuscript

IEEE ASME Trans Mechatron. Author manuscript; available in PMC 2021 December 17.

Published in final edited form as:

IEEE ASME Trans Mechatron. 2021 December ; 26(6): 2967–2976. doi:10.1109/tmech.2021.3049327.

Characterization of a packaged triboelectric harvester under simulated gait loading for total knee replacement

Nabid Aunjum Hossain[a], **Geofrey George Yamomo**[b], **Ryan Willing**[b], **Shahrzad Towfighian**[a,*]

[a]Binghamton University, 4400 Vestal Parkway E., Binghamton, NY

[b]University of Western Ontario, London, Canada

Abstract

Load sensing total knee replacement (TKR) implants are useful tools for monitoring prosthesis health and providing quantitative data to support patient claims of pain or instability. However, powering such devices throughout the entire life of the knee replacement is a challenge, and self-powered telemetry *via* energy harvesting is an attractive solution. In this study, we implemented vertical contact mode triboelectric energy harvesters inside a knee implant package to generate the power required for embedded digitization and communications circuitry. The harvesters produce small-scale electric power from physiologically relevant loads transmitted through the knee. Experiments were performed on a joint motion simulator with an instrumented package prototype between the polyethylene bearing and tibial tray. The amplitude and the pattern of the power output varied with the input loadings. Under sinusoidal loading the maximum apparent power harvested was around 7μW at (50–2000)N whereas, under vertical compressive gait loading the harvesters generated around 10μW at average human knee loads of (151–1950)N and 20μW when the maximum applied load was increased by 25%. Full six degrees of freedom (6-DoF) gait load/motions at 0.67Hz produced 50% less power due to the slower loading rate. The results show the potential of developing a triboelectric energy harvesting-based self-powered instrumented knee implant for long-term *in vivo* knee joint force measurement.

Index Terms

Knee implant package prototype; Triboelectric energy harvesting; Total knee replacement; *In vivo* force measurement; Joint motion simulator; Biomedical sensor

I. Introduction

Total knee replacement (TKR) is a common surgical treatment for end-stage knee osteoarthritis, performed over 600K times per year in the USA alone [1]–[3] and much of the surgeries is occurring in younger patients [4]. While generally considered a largely successful procedure for alleviating pain and restoring mobility, relatively high revision rates, and low patient satisfaction due to issues related to prosthesis component wear, loosening, and instability persist [5], [6]. These problems may all be symptoms of sub-

*Corresponding author: Shahrzad Towfighian is with the Department of Mechanical Engineering, Binghamton University, New York, 13902 USA, stowfigh@binghamton.edu.

Author Manuscript Author Manuscript Author Manuscript Author Manuscript

optimal load transfer across the tibiofemoral joint [7]; however, routine direct measurement of load transfer across the knee during activities of daily living is not part of the post-operative continuum of care for TKR patients. This is due to the lack of simple, low-cost, and commercially-available embedded sensors available for use in TKR implants.

Several embedded sensor systems have been developed to measure tibiofemoral forces. Kaufman *et al.* introduced the earliest instrumented implant device that had strain gauges to measure tibiofemoral forces *in vitro* [8]. The first reported usage of a sensor-embedded total knee implant in a patient was that of D'Lima *et al.* [9]–[11]. This device incorporated four load cells, and a wireless micro-transmitter to measure and transmit *in vivo* tibial forces. Bergmann et al. also published several in-depth analyses of knee forces and moments on five subjects using the similar concept of an instrumented knee implant [12]–[14]. These investigations from the D'Lima and the Bergmann group were groundbreaking in the field of instrumented tibial prosthesis. Their results showed the feasibility of long-term *in vivo* load measurements after a TKR surgery; however, the only real problem is that their designs were limited by the external coil power source. These instrumented implants were powered *via* inductive coupling with an external coil wrapped around the knee. This requirement could limit patient mobility, and prevents continuous (e.g. 24 hours) data collection.

Self-powered load sensors have recently been proposed as a solution for enabling continuous real-time measurement of joint loads, and have been described in previous studies. Electromagnetic induction is one of the methods of power generation that was integrated into the knee implant design by Luciano et al. [15]. However, this mechanism may degrade the implant functions and is not viable for different implant designs as it requires major changes to the structure of the implants. Piezoelectric (PZT) power harvesting has become a popular method for converting mechanical energy into usable electrical energy [16], [17]. Platt *et al.* demonstrated the feasibility of *in vivo* power generation from the deformation of PZT ceramics inserted on a tibial tray [18], [19]. Almouahed *et al.* presented a knee implant prototype that can harvest power, and identify the center of pressure from four piezoelectric transducers placed inside a modified knee implant [20], [21], and later, the prototype was optimized to a more power-efficient and biocompatible design [22]. However, such modification of the traditional implant design could lead to complications in performing the already developed surgical technique. In a recent study, Safaei *et al.* showed a similar concept of energy harvesting, and sensing from embedded PZT ceramics that did not require modifications into the implant design, and can be used with traditional, and FDA-approved tibial components [23]. Despite these promising works, the PZT ceramics have some drawbacks including non-biocompatibility, low power density, and complicated fabrication process (polarization at extremely low temperature) compared to some newer methods of energy harvesting.

Triboelectric energy harvesting is a relatively recent invention for converting mechanical motion to usable electrical energy that has a broad range of material selections, unlike the piezoelectric mechanism that is limited to few ceramics that often contain lead. It has been developed for a wide range of sensor applications, [24] including biomedical systems [25]. It generates electricity from the physical contact between two different materials through contact electrification and electrostatic induction. Although the contact

Author Manuscript Author Manuscript Author Manuscript Author Manuscript

electrification phenomena are known for thousands of years, the understanding of the concept remains elusive. The contact charging behavior of two materials depends on the intrinsic material properties such as the atomic surface structure and the external driving parameters such as contact force, humidity, surface contamination, and dielectric breakdown of air [26]. Moreover, friction plays a significant role in the charge generation process and also in the surface wears and stability of the output of a triboelectric system. The high friction coefficient is found beneficial for improving the electrical output of sliding-mode triboelectric generators [27]. Although not in the area of the triboelectric harvester, the frictional models on micro-motion systems [28] can be useful in modeling the frictional behavior in a sliding-mode triboelectric harvester. However, in a vertical contact-mode triboelectric harvester such as the harvesters used in this study, friction occurs between the micro-patterned surfaces when the layers engage in the vertical direction and are more difficult to model. Mechanical deformation at the contact surfaces also influences the charge generation and has been investigated in our previous works [29], [30].

High efficiency at low frequency, low cost, high power density ($313\,W/m^2$ [24]), and simple fabrication are some of the advantages of triboelectric energy harvesting over other methods [31] that convert mechanical impact [32], [33] or pressure to electricity. Triboelectric self-powered pressure sensors have been developed rapidly in recent years [34]–[36]. The triboelectric pressure sensors have a wider detection limit, better sensitivity, and greater stability than other existing pressure sensing technologies [37]. Because of these attributes, this technology has great potential for biomedical implants but has not received enough attention.

The idea of using a triboelectric generator/harvester (TEG) for powering a digitized circuit, and measuring the tibiofemoral forces, was first proposed by members of our group [38]. They also presented preliminary tests of a biocompatible triboelectric harvester inserted between a UHMWPE bearing and a tibial tray under gait loading [39], [40]. However, the preliminary designs [38]–[40] need significant improvements in several aspects. In this study, a new packaged harvester design is introduced, which can address some of the major drawbacks of our previous studies. The proposed harvester design has an optimized shape for the TKR as it closely follows the shape of the tibial tray. The new tibial-shaped harvester generates more power compared to the previous design that had a rectangular shape. More specifically, the proposed packaged harvesters can generate more power with less amount of load transmitting through the PDMS layer. It is possible because the package is innovatively designed for higher stiffness, and the harvesters have an optimal surface area that more effectively uses the available spaces on a tibial tray. Moreover, the previous prototypes lacked a proper package design for housing the harvester layers. The rubber springs used in between the harvester layers failed under average gait loads and led to the harvester damage in excessive loads. The Ti package made of Ti6Al4V used in this study is properly designed to be strong enough against shear forces (prevent sliding) and 6-DOF gait loads. It has a fatigue strength of 550 MPa and stiffness of 3190 N/mm [41]. Herein, two tibial-shaped TEG configurations were installed in a package prototype and tested on a joint motion simulator. This was the first attempt to evaluate the performance of triboelectric harvester output inside a package prototype, designed for versatile commercial knee implants. We experimentally measured the power output of the harvesters across external resistance under

Author Manuscript Author Manuscript Author Manuscript Author Manuscript

varying sinusoidal and human walking gait loads. We also investigated the effect of a parallel connection between the harvesters by conducting separate experiments on each harvester.

II. Materials and methods

A. Package prototype

A tibial tray shaped package with elastic materials located along the periphery is required to encapsulate the TEGs, and the accompanying electronics for data acquisition, data transmission, and energy storage. Based on the TEG's working mechanism that is dependent on the contact and separation of triboelectric materials, the package provides a net deflection of 0.2 mm at the maximum compressive load in the gait cycle (2600 N) while not exceeding the fatigue limit of the Ti6Al4V (550 MPa) [42]. We hypothesize that this small amount of deflection under load due to the compliance of the package would not be enough to have any noticeable effect on the patient's gait. Future human cadaver testing can verify this assumption. The elastic materials, along the periphery, undertook the shape of a series of stacked beams. Based on a size 7 Stryker Triathlon Knee System (Stryker, Kalamazoo, MI), the interlocking mechanism was reverse engineered on the inferior and superior surfaces of the package. The package prototype was manufactured by selective laser melting (SLM) using the Renishaw AM 400 (Wotton-under- Edge, UK). Ti6Al4V was used because of its biocompatibility, and relatively lower modulus of elasticity when compared with other metal alloys. A side view of the package prototype is shown in Figure 1(d). The current prototype adds approximately 16 mm to the overall height of the tibial component. The prototypical nature of the current iteration required increased thickness that we can reduce in future iterations. Furthermore, the overall thickness can be reduced by using the thinnest possible poly bearings from the currently available ranges (9 mm to 19 mm) in the Triathlon system.

B. Harvester-package configuration and assembly

One of the challenging tasks of this study was to fit two triboelectric harvester parts inside of the package prototype for economic, and optimum use of the housing spaces. The harvester parts were designed to closely follow the contour of the tibial tray. In Figure 1, 3D design views of the harvesters and the package are demonstrated. With this design, the harvesters can generate power over $5\mu W$, and the area requirement (around $1cm^2$) for a digitized circuit of the sensory systems necessary for signal processing, and data logging of a smart knee implant [38]. The vertical contact mode triboelectric harvesters used in this study consist of two major parts, an upper Titanium (Ti) electrode, and a lower polydimethylsiloxane (PDMS) insulator coated on another Ti layer that acts as a back electrode. PDMS and Ti were chosen because both are biocompatible, and they make a suitable triboelectric pair for power generation. The electrodes were CNC machined in two opposite orientations from 0.5mm thick Ti plates at Progressive Tool Co. Endicott, NY. The surface area of a left- and a right-oriented electrode is $9.5cm^2$ and $9.2cm^2$ respectively. The upper Ti electrodes have micropatterned surfaces ($100\mu m$ sawtooth ridges), and the lower PDMS layers are spin-coated on a flat and a patterned Ti electrode. PDMS was fabricated following the same process described in our previous work [30] and the thicknesses of the PDMS layers are in the range of 180 – $200\mu m$. Two harvester configurations were made with the upper Ti

Author Manuscript Author Manuscript Author Manuscript Author Manuscript

electrodes part facing a reverse oriented (i) flat, and (ii) patterned PDMS-Ti electrode for the lower part.

For each configuration, a right- and a left-oriented harvester were assembled in the medial, and the lateral side of the package compartment. The assemblies were created such that when knee-motion force was transmitted, the upper Ti electrode and the lower PDMS layer had enough contact to generate the power needed for the sensing application. To accomplish this, two $1.5mm$ plastic spacers on the inside compartment, and one $0.25mm$ and one $0.1mm$ plastic spacer on the inner surface of the lid were mounted. Then, the upper, and the lower electrodes were wired on their backside for connection purposes and attached to the spacers. These spacers were used to reduce the gap required between the upper and the lower tribolayers to generate the power demanded by the frontend electronic system of the smart knee implant [43]. Moreover, these plastic spacers act as an electrical insulator between the Ti package, and the harvester parts. The important parameters such as the device area, gap between the upper and lower tribolayers, size and shape of the micro-patterns, the thickness of the dielectric layer, and the external resistance were kept the same to the best of our ability for each harvester. Figure 2 (a–d) shows the components and their arrangement in building up the final assembly used in the experiments.

C. Experimental setup

The harvester-package prototypes were tested on a six-degrees-of-freedom (6-DoF) servo-hydraulic joint motion simulator (AMTI VIVO, Watertown, MA, USA). Several experiments were performed using the two types of harvester-package assemblies. The harvester configurations for these assembly types are illustrated in Figure 3 (b). As shown in Figure 3 (a) each assembly was mounted in between the tibial tray, and the UHMWPE bearing. A size 7 tibial tray (Triathlon, TKR Stryker, Kalamazoo, MI) was secured to a custom fixture connected to the lower actuator of the AMTI VIVO joint simulator using dental cement (Dentstone, Kulzer, LLC, South Bend, IN). A size 7 femoral component was affixed to a femoral component holder designed to interface with the abduction arm of the AMTI VIVO joint simulator using polymethylmethacrylate (PMMA) cement (Bosworth Fastray, Keystone Industries, Myerstown, PA). The energy harvesting system was fully assembled by interlocking a 9 mm thick condylar stabilized (CS) UHMWPE bearing to the superior surface of the prototype. The harvesters were connected with a $220M\Omega$ external resistance in parallel for all the experiments except for the one TEG experiments (section III-B) when each harvester was measured individually. The voltage and the current outputs from the harvesters were measured with Keithley 6514 electrometer. Apparent power outputs are calculated by multiplying RMS voltage with corresponding RMS current results for Figure 6, 7, and 9. Since current results for the sinusoidal experiment on flat PDMS harvester were not measured, RMS powers (V^2/R) are calculated for Figure 5. A schematic of the experimental setup is shown in Figure 4.

Most of the experiments of this study were performed using the compression gait cycle (1-DOF gait) of the joint simulator. It is referred as 1-DOF gait in the rest of the paper. The other degrees of freedom such as anteroposterior translation (AP), mediolateral translation (ML), internal-external rotation (IE), and abduction-adduction (AA) maintained a load of $0N$

Author Manuscript Author Manuscript Author Manuscript Author Manuscript

or $0 Nm$ while the flexion degree of freedom was set to 0^0. Nevertheless, one assembly was tested under a 6-DoF gait with the same experimental setup, to compare the electrical output results between 6-DoF and 1-DOF gait. The simulated gait loads used in this study were based on previously measured tibiofemoral loads [14].

The harvester-package prototype assemblies were further tested under varying magnitudes of sinusoidal, and gait cyclic motions. While the minimum of the sine forces was kept constant at $50 N$ for the Ti6Al4V package-harvester assemblies, the maximum sinusoidal force was varied from $400 N$ to $2000 N$. For gait cyclic experiments, the previously reported average minimum-maximum knee loads of $(151 – 1950) N$ from human walking motions were applied. Additionally, experiments were conducted for a 25% increase and a 25% reduction of the minimum and maximum gait loads.

III. Results

A. Effect of input loads and motions

The effects of different types of input loads and motions on the performance of the Ti6Al4V package-harvester configurations (Figure 3) are presented here. The RMS power outputs at various maximum sinusoidal loads are shown in Figure 5. Increment of maximum load $(400 – 2000) N$ had statistical significant ($p < 0.05$; $t – test$) effect on the harvesters' power output $(0.1 - 7) \mu W$. The power consumption of a previously designed frontend electronic system is approximately $5.35 \mu W$ [43], which enables exclusive powering from the harvester at $2000 N$. Although there is statistical significant ($p < 0.05$; $t - test$) difference between the output from the two harvester configurations, it does not follow a linear trend for the sinusoidal experiment.

The 1-DOF gait variation results are illustrated in Figure 6. It shows a quantitative analysis of the apparent power output for the 25% increment, and the reduction of the minimum and the maximum of the gait loads from walking. While the highest apparent power of $20 \mu W$ was measured for the harvester configuration with flat PDMS at $151 – 2437 N$, the lowest apparent power of $5 \mu W$ was found for the harvester configuration with patterned PDMS at $151 – 1462 N$.

The six-degrees-of-freedom simulator creates closer to the real gait cycle. The performance of the Ti6Al4V package-harvester setup under a 1-DOF and a 6-DoF gait test are depicted in Figure 7. The power output under the 6-DoF gait was almost 50% less than the power output from the 1-DOF gait test. For 6-DoF gait (Figure 8b), the loads on the package were transmitted via 3 translations and 3 rotations at $0.67 Hz$, and for 1-DOF gait (Figure 8a), the same amount of loads were applied at 1Hz in the vertical direction only. The corresponding RMS voltage recorded was $36.97 V$, and $29.42 V$ for 1-DOF, and 6-DoF gait, respectively (Figure 8c, Figure 8d). The corresponding RMS current recorded was $0.23 \mu A$, and $0.15 \mu A$ for 1-DOF, and 6-DoF gait, respectively (Figure 8e, Figure 8f).

B. Effect of parallel connection

At 151 − 1950 N of 1-DOF gait loading, the generators at the medial and the lateral side of the package compartment for each Ti6Al4V package-harvester assembly were

Author Manuscript Author Manuscript Author Manuscript Author Manuscript

tested separately with a 220MΩ external resistance. As shown in Figure 9, the apparent power outputs from these individual tests are distinct and consistent for the two harvester configurations. Under the same 1-DOF gait and the same experimental setup, two TEGs in parallel connection produced more power than one TEG generated on average for each configuration. The apparent power harvested from two harvesters in parallel connection is 2.9, and 2.5 times higher than the average single harvester output for the flat, and the patterned PDMS harvester configuration, respectively. The reason for higher output is that when two such generators are connected in parallel, the output current is increased by some amount that depends on the internal impedance of the harvesters and the load resistance of the circuit. The circuit analysis for single, parallel, and series connection are included in the Appendix. It proves that the current and power output across the load resistance for two TEGs in parallel is higher than a single TEG.

IV. Discussion and conclusions

In this study, we integrated two vertical contact mode triboelectric energy harvester configurations into a 3D printed package for measuring tibiofemoral forces in knee implants. Two identical harvesters from each configuration were assembled inside the medial and the lateral side of the package compartment of the Ti6Al4V package and placed between the UHMWPE bearing and the tibial tray of the AMTI VIVO joint motion simulator. Each assembly was tested under different sinusoidal and walking gait loads. The statistical difference observed in the apparent power output with varying loads between the patterned and the flat PDMS harvester configuration was below our expectation. Although patterned PDMS should increase the contact surfaces [36] and produce larger outputs, it generated slightly less power than the flat PDMS harvester at most sinusoidal and all 1-DOF gaits. This can be due to the fact that the patterned surfaces of Ti and PDMS are not aligned, which causes a random engagement of the two surfaces, and can ultimately cause smaller output. The perfect alignment of two micro patterned surfaces is cumbersome; may deviate over time, and is not advised for total knee replacement applications. As a result our comparison on the patterned PDMS, and flat PDMS harvester does not follow the expected trends.

For 1-DOF gait experiments, increasing the maximum load always significantly ($p < 0.05$; $t-test$) increased the output of the harvester. The minimum load correlates to the initial separation distance between the two layers of each generator. A lower minimum value shows a larger initial gap, which should result in higher output because of the capacitive effect of the harvester. However, we see the highest output is achieved for the minimum loads of 113 N, 189 N, and 151 N, respectively, which do not follow the expected trend. Although these changes in the initial gap were not measured experimentally; it is possible that, the gaps were below and above an optimum. This conclusion is based on our previous work that showed a gap for which a vertical contact mode TEG produces the maximum power [40]. That is why the power output in this study did not vary linearly for the different minimum and the same maximum gait loads.

The apparent power output recorded under the average 1-DOF gait of $151-1950N$ at $1Hz$ were around $10\mu W$, which is almost twice the power consumption of 5.32 μW of a

Author Manuscript Author Manuscript Author Manuscript Author Manuscript

previously designed frontend electronic system for the harvester [43]. This property enables powering the processing circuit entirely from the gait loading, and assures a self-powered system. The harvester-package setup generated even more power at higher gait loads. Moreover, we expect the power to get increased at higher frequencies [38]. Our testing using the 6-DoF gait had less output than the 1-DOF gait mainly because of lower frequency selection for the 6-DoF gait test. At lower frequency, the amount of the surface contact between the tribolayers of the harvesters at a given time was less in 6-DoF gait compared to the 1-DOF gait. Since the surface charge density of a triboelectric generator is directly proportional to the surface contact area up to a saturation limit [30], the harvesters under 6-DoF gait generated less power than the harvesters under 1-DOF gait. However, we believe the harvesters can generate enough power (around $5\mu W$) required for running a digitization circuitry of a sensor system.

In the future, we will implement a sensor system into the available space inside the harvester-package assembly, and test the *in vitro* characteristics of the energy harvesting, and the sensing system for simulated activities of daily living.

Some of the limitations of the proposed device are as follows:

1. Current methods of harvester installation into the package is lacking perfection. The installation method should be more managed to allow control over the gap between harvester layers inside the package.
2. It is reported in the literature that, the gap between the tribolayers has effects on the harvesters' output. However, it was not possible to measure the gaps once the harvesters were installed and set for the experiments. Thus, lack of knowledge about the gap in each of the harvesters in the package compartment, is another limitation of this study. Moreover, current procedure of using spacers to reduce the gap is not accurate enough to obtain an optimum gap.
3. The surface of the PDMS layers can be damaged from dynamic contact with the upper Titanium electrode. The current design is more durable compared to our previous works because of stronger package design. However, the reliability and the robustness of the current system will be tested in our future work by testing under millions of cycles. Although by improving the package strength in the current design, risks of failure have been reduced significantly, it is not resilient against failures such as damage of package/harvester materials in the system [44].
4. The current design needs to be optimized. Because a more compliant design with a similar energy harvesting system can improve the efficiency of the system. However, there is a trade-off limit between the strength and durability of a compliant mechanism that can be determined from experiments or mathematical modeling such as the topology optimization technique [45].

Acknowledgment

This research has been supported by the National Institute of Arthritis and Musculoskeletal and Skin Diseases of the National Institute of Health under award number R21AR068572. The content is solely the responsibility of the

Author Manuscript Author Manuscript Author Manuscript Author Manuscript

authors and does not necessarily represent the official views of the National Institute of Health. The authors greatly appreciate Progressive Tool Company that made the Titanium parts.

Appendix

The electrical model for a triboelectric harvester can be analyzed following Niu et al. [46]. The behavior of such harvester is modeled with three circuit elements: an ac source voltage V_M, a variable capacitor C_M, and an internal resistance r. The variable capacitor C_M and the internal resistance r are the components of the source impedance Z. In Figure 10 the lumped-parameter electrical model of the triboelectric harvester for three different circuit connections are shown. The theoretical power output across the load resistance R for each of the circuit model is derived here.

For one TEG with an external load resistance (Figure 10a) the power output across R is,

$$P_{0,\,single} = I^2 R \tag{1}$$

Applying KVL, the current I can be obtained as:

$$\begin{aligned} IZ + IR + V_M &= 0 \\ I &= -\frac{V_M}{R+Z} \end{aligned} \tag{2}$$

From equation 1 and 2,

$$P_{0,\,single} = \left|\frac{1}{R+Z}\right|^2 V_M^2 R \tag{3}$$

For two TEGs in parallel with an external load resistance (Figure 10b) the power output across R is,

$$P_{0,\,parallel} = I_R^2 R \tag{4}$$

$$\text{At node o, } I_R = I_1 + I_2 \tag{5}$$

Applying KVL in loop 1 an 2 the following two equations can be obtained,

$$-V_{M1} - I_1 Z_1 + I_2 Z_2 + V_{M2} = 0 \tag{6}$$

$$-V_{M2} - I_2 Z_2 - I_R R = 0 \tag{7}$$

Let $V_{M1} = V_{M2} = V_M$, $Z_1 = Z_2 = Z$ as the harvesters are identical. Thus, equation 5, 6 & 7 can be written in following matrix format.

Author Manuscript Author Manuscript Author Manuscript Author Manuscript

$$\begin{bmatrix} -Z & Z \\ R & R+Z \end{bmatrix} \begin{Bmatrix} I_1 \\ I_2 \end{Bmatrix} = \begin{Bmatrix} 0 \\ -V_M \end{Bmatrix} \tag{8}$$

Solving equation 8, I_1 and I_2 can be obtained as:

$$\begin{Bmatrix} I_1 \\ I_2 \end{Bmatrix} = \begin{Bmatrix} -\dfrac{V_M}{2R+Z} \\ -\dfrac{V_M}{2R+Z} \end{Bmatrix} \tag{9}$$

From equation 5 and 9,

$$I_R = -\frac{2V_M}{2R+Z} \tag{10}$$

From equation 4 and 10,

$$P_{0,\ parallel} = \left|\frac{1}{2R+Z}\right|^2 4V_M^2 R \tag{11}$$

For two TEGs in series with an external load resistance (Figure 10c) the power output across R is,

$$P_{0,\ series} = I^2 R \tag{12}$$

Applying KVL, the current I can be obtained as:

$$\begin{aligned} -V_{M1} - IZ_1 - V_{M2} - IZ_2 - IR = 0 \\ I = -\frac{V_{M1} + V_{M1}}{R + Z_1 + Z_2} \end{aligned} \tag{13}$$

Set $V_{M1} = V_{M2} = V_M$, $Z_1 = Z_2 = Z$ in equation 13

$$I = -\frac{2V_M}{R+2Z} \tag{14}$$

From equation 12 and 14,

$$P_{0,\ series} = \left|\frac{1}{R+2Z}\right|^2 4V_M^2 R \tag{15}$$

Set the impedance as

Author Manuscript Author Manuscript Author Manuscript Author Manuscript

$$Z = r + \frac{1}{j\omega C_M} = r - j\frac{1}{\omega C_M}$$

and rewrite the power expressions.

From Equation 3,

$$P_{0,\ single} = \left|\frac{1}{(R+r) - j\left(\frac{1}{\omega C_M}\right)}\right|^2 V_M^2 R = \frac{V_M^2 R}{(R+r)^2 + \frac{1}{(\omega C_M)^2}} \tag{16}$$

From Equation 11,

$$P_{0,\ parallel} = \left|\frac{1}{(2R+r) - j\left(\frac{1}{\omega C_M}\right)}\right|^2 4V_M^2 R = \frac{4V_M^2 R}{(2R+r)^2 + \frac{1}{(\omega C_M)^2}} \tag{17}$$

From Equation 15,

$$P_{0,\ series} = \left|\frac{1}{(R+2r) - j\left(\frac{2}{\omega C_M}\right)}\right|^2 4V_M^2 R = \frac{4V_M^2 R}{(R+2r)^2 + \frac{4}{(\omega C_M)^2}} \tag{18}$$

According to the equation 16,17 and 18, the power output from two TEGs in parallel connection is larger than the single and the series connection. The actual numerical differences in these three outputs depend on the load and internal resistance variables. Based on the impedance matching, the two TEGs in parallel can provide up to some x the power of a single harvester. If two resistances are equal, the power increment in the parallel connection will reach close to 4x times. However, if the two resistances are not equal, this power increment will be reduced to a number less than 4x. These theoretical results of power increment are also found in the experimental results (Figure 9). Although we assumed that the selected load resistance and the internal resistance were equal in the experiment, the highest power increment recorded in a parallel connection was 2.9x times the single connection. Thus, our impedance matching analysis might not be perfect, and this power

Author Manuscript Author Manuscript Author Manuscript Author Manuscript

increment can be enhanced more close to 4x times by more accurate impedance matching in the parallel circuit.

Biographies

Nabid Aunjum Hossain received his B.S. degree in mechanical engineering from the Bangladesh University of Engineering and Technology (BUET), Dhaka, Bangladesh, in 2016. In 2017 he joined the mechanical engineering department of SUNY Binghamton, Binghamton, NY, USA, where he has been working towards his PhD degree. His research interests are in electro-mechanical systems, vibration and energy harvesting. Currently his focus is on developing a triboelectric energy harvesting based, self-powered instrumented knee implant.

Geofrey Yamomo received his BESc and MESc degrees in mechanical engineering from the University of Western Ontario in London, Ontario, Canada in 2017 and 2020, respectively. His research work covered the design and analysis of orthopaedic implants. He is a member of the Canadian Society for Mechanical Engineering (CSME).

Ryan Willing completed his PhD in Mechanical Engineering at Queen's University in 2010 and a post-doc at Western University in 2013. He is an Assistant Professor in Mechanical and Materials Engineering and Biomedical Engineering at Western University, a member of Western's Bone and Joint Institute, and a Scientist with the Lawson Health Research Institute.

Author Manuscript Author Manuscript Author Manuscript Author Manuscript

Dr. Shahrzad Towfighian Shahrzad Towfighian received the B.S. degree from the Amirkabir University of Technology, Iran, in 2001, the M.S. degree from Ryerson University, Canada, in 2006, and the Ph.D. degree from the University ofWaterloo, Canada, in 2011. She joined the Mechanical Engineering Department, State University of New York at Binghamton, in Fall 2013. Her research interests are microelectromechanical systems and energy harvesting for bio-medical devices. She focuses on creating theoretical and experimental frameworks to explain the underlying mechanism of electro-mechanical systems. Using these frameworks, she seeks innovative methods to improve functionality of devices for various applications. She was a recipient of several grants from the National Science Foundation and the National Health Institute.

References

[1]. Kremers HM, Larson DR, Crowson CS, Kremers WK, Washington RE, Steiner CA, Jiranek WA, and Berry DJ, “Prevalence of total hip and knee replacement in the United States,” The Journal of bone and joint surgery. American volume, vol. 97, no. 17, p. 1386, 2015. [PubMed: 26333733]

[2]. Weinstein AM, Rome BN, Reichmann WM, Collins JE, Burbine SA, Thornhill TS, Wright J, Katz JN, and Losina E, “Estimating the burden of total knee replacement in the United States,” The Journal of bone and joint surgery. American volume, vol. 95, no. 5, p. 385, 2013. [PubMed: 23344005]

[3]. Jain NB, Higgins LD, Ozumba D, Guller U, Cronin M, Pietrobon R, and Katz JN, “Trends in epidemiology of knee arthroplasty in the United States, 1990–2000,” Arthritis & Rheumatism, vol. 52, no. 12, pp. 3928–3933, 2005. [PubMed: 16320340]

[4]. Kurtz SM, Lau E, Ong K, Zhao K, Kelly M, and Bozic KJ, “Future young patient demand for primary and revision joint replacement: national projections from 2010 to 2030,” Clinical Orthopaedics and Related Research®, vol. 467, no. 10, pp. 2606–2612, 2009. [PubMed: 19360453]

[5]. Sharkey PF, Lichstein PM, Shen C, Tokarski AT, and Parvizi J, “Why are total knee arthroplasties failing today—has anything changed after 10 years?” The Journal of arthroplasty, vol. 29, no. 9, pp. 1774–1778, 2014. [PubMed: 25007726]

[6]. Suarez J, Griffin W, Springer B, Fehring T, Mason JB, and Odum S, “Why do revision knee arthroplasties fail?” The Journal of arthroplasty, vol. 23, no. 6, pp. 99–103, 2008. [PubMed: 18538534]

[7]. Dorr LD and Boiardo RA, “Technical considerations in total knee arthroplasty.” Clinical orthopaedics and related research, no. 205, pp. 5–11, 1986.

[8]. Kaufman KR, Kovacevic N, Irby SE, and Colwell CW, “Instrumented implant for measuring tibiofemoral forces,” Journal of biomechanics, vol. 29, no. 5, pp. 667–671, 1996. [PubMed: 8707796]

[9]. D’Lima DD, Patil S, Steklov N, Slamin JE, and Colwell CW Jr, “Tibial forces measured in vivo after total knee arthroplasty,” The Journal of arthroplasty, vol. 21, no. 2, pp. 255–262, 2006. [PubMed: 16520216]

[10]. D’Lima DD, Patil S, Steklov N, Chien S, and Colwell CW Jr, “In vivo knee moments and shear after total knee arthroplasty,” Journal of biomechanics, vol. 40, pp. S11–S17, 2007. [PubMed: 17462659]

Author Manuscript Author Manuscript Author Manuscript Author Manuscript

[11]. Kirking B, Krevolin J, Townsend C, Colwell CW Jr, and D'Lima DD, "A multiaxial force-sensing implantable tibial prosthesis," Journal of biomechanics, vol. 39, no. 9, pp. 1744–1751, 2006. [PubMed: 16023656]

[12]. Kutzner I, Heinlein B, Graichen F, Bender A, Rohlmann A, Halder A, Beier A, and Bergmann G, "Loading of the knee joint during activities of daily living measured in vivo in five subjects," Journal of biomechanics, vol. 43, no. 11, pp. 2164–2173, 2010. [PubMed: 20537336]

[13]. Kutzner I, Trepczynski A, Heller MO, and Bergmann G, "Knee adduction moment and medial contact force–facts about their correlation during gait," PloS one, vol. 8, no. 12, 2013.

[14]. Bergmann G, Bender A, Graichen F, Dymke J, Rohlmann A, Trepczynski A, Heller MO, and Kutzner I, "Standardized loads acting in knee implants," PloS one, vol. 9, no. 1, 2014.

[15]. Luciano V, Sardini E, Serpelloni M, and Baronio G, "Analysis of an electromechanical generator implanted in a human total knee prosthesis," in 2012 IEEE Sensors Applications Symposium Proceedings. IEEE, 2012, pp. 1–5.

[16]. Anton SR and Sodano HA, "A review of power harvesting using piezoelectric materials (2003–2006)," Smart materials and Structures, vol. 16, no. 3, p. R1, 2007.

[17]. Yang W and Towfighian S, "A parametric resonator with low threshold excitation for vibration energy harvesting," Journal of Sound and Vibration, vol. 446, pp. 129–143, 2019.

[18]. Platt SR, Farritor S, Garvin K, and Haider H, "The use of piezoelectric ceramics for electric power generation within orthopedic implants," IEEE/ASME transactions on mechatronics, vol. 10, no. 4, pp. 455–461, 2005.

[19]. Platt SR, Farritor S, and Haider H, "On low-frequency electric power generation with PZT ceramics," IEEE/ASME transactions on Mechatronics, vol. 10, no. 2, pp. 240–252, 2005.

[20]. Almouahed S, Gouriou M, Hamitouche C, Stindel E, and Roux C, "Design and evaluation of instrumented smart knee implant," IEEE Transactions on Biomedical Engineering, vol. 58, no. 4, pp. 971–982, 2010. [PubMed: 20639169]

[21]. Almouahed CHESS, Gouriou M and Roux C, "The use of piezoceramics as electrical energy harvesters within instrumented knee implant during walking," IEEE/ASME Transactions on Mechatronics, vol. 16, no. 5, pp. 799–807, 2011.

[22]. Almouahed S, Hamitouche C, Stindel E, and Roux C, "Optimization of an instrumented knee implant prototype according to in-vivo use requirements," in 2013 IEEE Point-of-Care Healthcare Technologies (PHT). IEEE, 2013, pp. 5–8.

[23]. Safaei M, Meneghini RM, and Anton SR, "Energy harvesting and sensing with embedded piezoelectric ceramics in knee implants," IEEE/ASME Transactions on Mechatronics, vol. 23, no. 2, pp. 864–874, 2018. [PubMed: 30853785]

[24]. Wang ZL, "Triboelectric nanogenerators as new energy technology for self-powered systems and as active mechanical and chemical sensors," ACS nano, vol. 7, no. 11, pp. 9533–9557, 2013. [PubMed: 24079963]

[25]. Zheng Q, Shi B, Li Z, and Wang ZL, "Recent progress on piezoelectric and triboelectric energy harvesters in biomedical systems," Advanced Science, vol. 4, no. 7, p. 1700029, 2017. [PubMed: 28725529]

[26]. Lacks DJ and Sankaran RM, "Contact electrification of insulating materials," Journal of Physics D: Applied Physics, vol. 44, no. 45, p. 453001, 2011.

[27]. Zhang W, Diao D, Sun K, Fan X, and Wang P, "Study on friction-electrification coupling in sliding-mode triboelectric nanogenerator," Nano Energy, vol. 48, pp. 456–463, 2018.

[28]. Liu Y, Li J, Zhang Z, Hu X, and Zhang W, "Experimental comparison of five friction models on the same test-bed of the micro stick-slip motion system," Mechanical Sciences, vol. 6, no. 1, p. 15, 2015.

[29]. Jin C, Kia DS, Jones M, and Towfighian S, "On the contact behavior of micro-/nano-structured interface used in vertical-contact-mode triboelectric nanogenerators," Nano Energy, vol. 27, pp. 68–77, 2016.

[30]. Hossain NA, Razavi MJ, and Towfighian S, "Analysis of mechanical deformation effect on the voltage generation of a vertical contact mode triboelectric generator," Journal of Micromechanics and Microengineering, 2020.

Author Manuscript Author Manuscript Author Manuscript Author Manuscript

[31]. Wang ZL, “On Maxwell’s displacement current for energy and sensors: the origin of nanogenerators,” Materials Today, vol. 20, no. 2, pp. 74–82, 2017.

[32]. Ibrahim A, Ramini A, and Towfighian S, “Experimental and theoretical investigation of an impact vibration harvester with triboelectric transduction,” Journal of Sound and Vibration, vol. 416, pp. 111–124, 2018.

[33]. Nelson D, Ibrahim A, and Towfighian S, “Dynamics of a threshold shock sensor: Combining bi-stability and triboelectricity,” Sensors and Actuators A: Physical, vol. 285, pp. 666–675, 2019.

[34]. Seol M-L, Lee S-H, Han J-W, Kim D, Cho G-H, and Choi Y-K, “Impact of contact pressure on output voltage of triboelectric nanogenerator based on deformation of interfacial structures,” Nano Energy, vol. 17, pp. 63–71, 2015.

[35]. Lin L, Xie Y, Wang S, Wu W, Niu S, Wen X, and Wang ZL, “Triboelectric active sensor array for self-powered static and dynamic pressure detection and tactile imaging,” ACS nano, vol. 7, no. 9, pp. 8266–8274, 2013. [PubMed: 23957827]

[36]. Fan F-R, Lin L, Zhu G, Wu W, Zhang R, and Wang ZL, “Transparent triboelectric nanogenerators and self-powered pressure sensors based on micropatterned plastic films,” Nano letters, vol. 12, no. 6, pp. 3109–3114, 2012. [PubMed: 22577731]

[37]. Rasel MS, Maharjan P, Salauddin M, Rahman MT, Cho HO, Kim JW, and Park JY, “An impedance tunable and highly efficient triboelectric nanogenerator for large-scale, ultra-sensitive pressure sensing applications,” Nano Energy, vol. 49, pp. 603–613, 2018.

[38]. Ibrahim A, Jain M, Salman E, Willing R, and Towfighian S, “A smart knee implant using triboelectric energy harvesters,” Smart Materials and Structures, vol. 28, no. 2, p. 025040, 2019. [PubMed: 31258261]

[39]. Ibrahim A, Yamomo G, Willing R, and Towfighian S, “Analysis of a triboelectric energy harvester for total knee replacements under gait loading,” in Active and Passive Smart Structures and Integrated Systems XII, vol. 10967. International Society for Optics and Photonics, 2019, p. 109671D.

[40]. Ibrahim A, Yamomo G, Willing T. Ryan, and Shahrzad, “Parametric Study of Triboelectric Transducer in Total Knee Replacement Application,” Journal of Intelligent Material Systems and Structures, 2020.

[41]. Yamomo G, “Design and Analysis of a Compliant 3D Printed Energy Harvester Package for Knee Implants,” Electronic Thesis and Dissertation Repository. 6728, https://ir.lib.uwo.ca/etd/6728.

[42]. Teoh S, “Fatigue of biomaterials: a review,” International journal of fatigue, vol. 22, no. 10, pp. 825–837, 2000.

[43]. Jain M, Ibrahim A, Salman E, Stanacevic M, Willing R, and Towfighian S, “Frontend Electronic System for Triboelectric Harvester in a Smart Knee Implant,” in 2019 IEEE 62nd International Midwest Symposium on Circuits and Systems (MWSCAS). IEEE, 2019, pp. 386–389.

[44]. Zhang W and Van Luttervelt C, “Toward a resilient manufacturing system,” CIRP annals, vol. 60, no. 1, pp. 469–472, 2011.

[45]. Cao L, Dolovich AT, Chen A, and Zhang WC, “Topology optimization of efficient and strong hybrid compliant mechanisms using a mixed mesh of beams and flexure hinges with strength control,” Mechanism and Machine Theory, vol. 121, pp. 213–227, 2018.

[46]. Niu S, Zhou YS, Wang S, Liu Y, Lin L, Bando Y, and Wang ZL, “Simulation method for optimizing the performance of an integrated triboelectric nanogenerator energy harvesting system,” Nano Energy, vol. 8, pp. 150–156, 2014.

Author Manuscript Author Manuscript Author Manuscript Author Manuscript

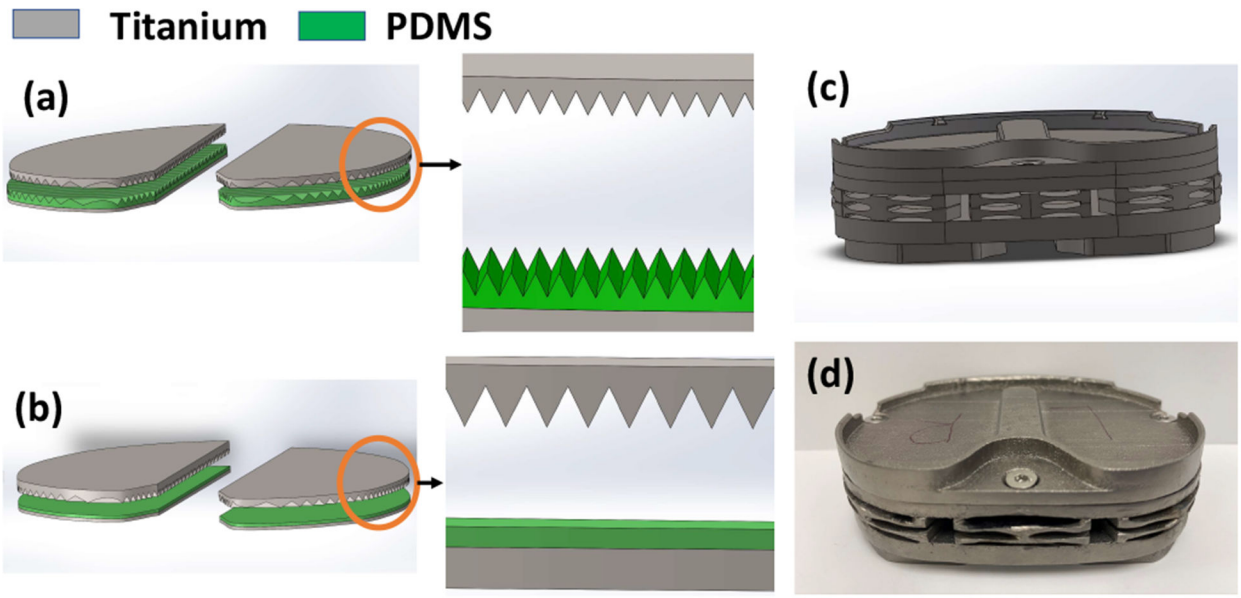

Fig. 1.

3D design view of harvesters and packages. (a) Harvester configuration with patterned PDMS. (b) Harvester configuration with flat PDMS. (c) Design view of Titanium(Ti6Al4V) package. (d) Fabricated real view of the Titanium(Ti6Al4V) package.

Author Manuscript Author Manuscript Author Manuscript Author Manuscript

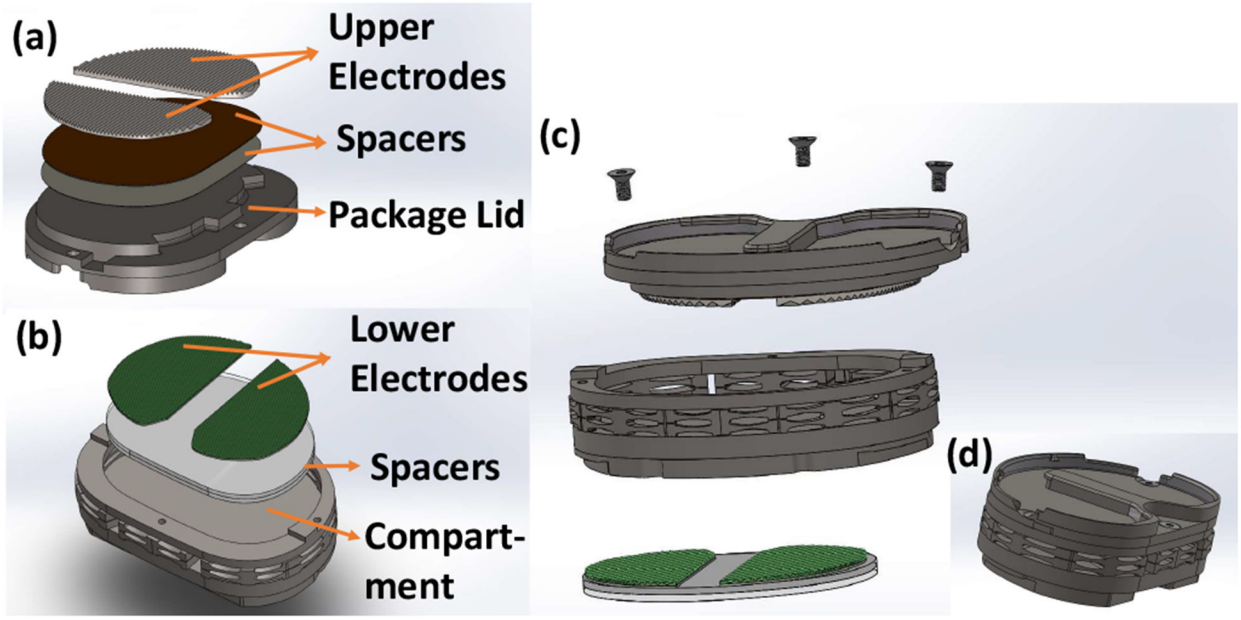

Fig. 2.

Assembly of two harvester configurations inside the package. (a) Attachment of the upper tribo-parts to the package lid. (b) Setup of the lower tribo-parts inside the package compartment. (c) An exploded view of the assembly parts. (d) Assembly view after fittings of the harvester inside the package.

Author Manuscript Author Manuscript Author Manuscript Author Manuscript

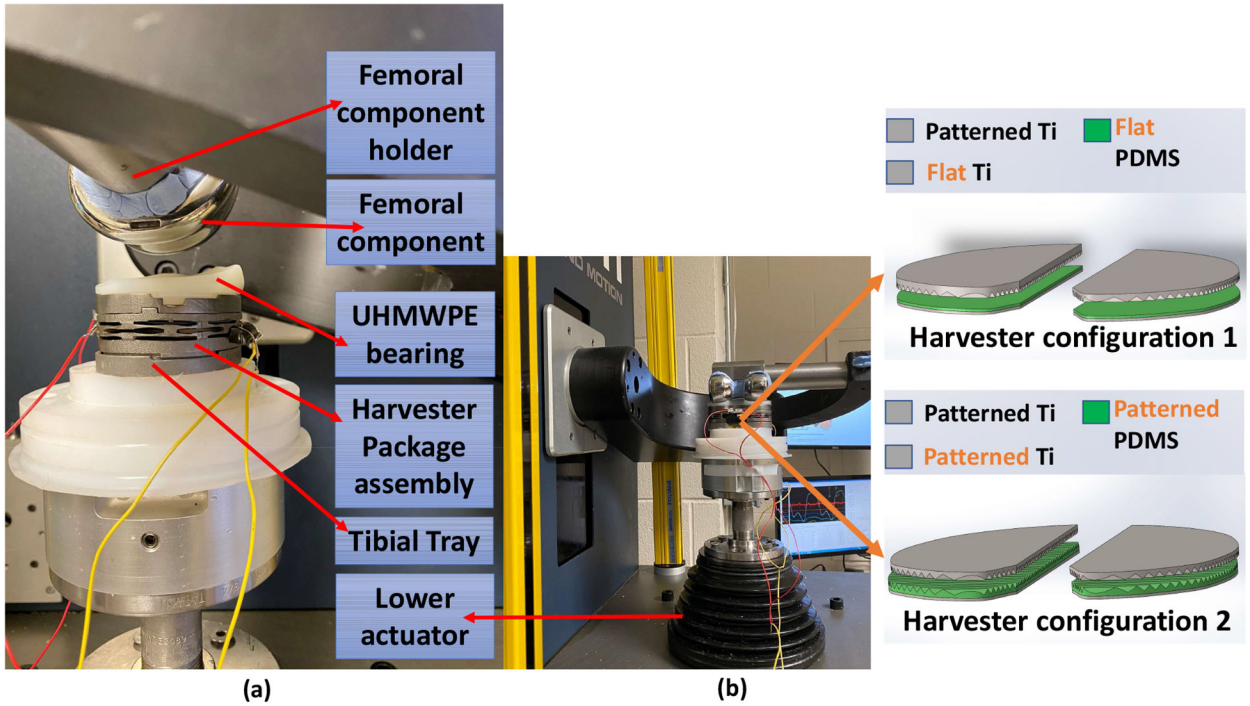

Fig. 3.

(a) Mounting of a harvester package assembly on the VIVO joint motion simulator. (b) Ti6Al4V made package prototype and two harvester configurations setup on the simulator. Configurations 1 and 2 contain a Ti layer coated with a flat and a patterned PDMS layer at the bottom, respectively. The top layer of the two is the same patterned Ti layer.

Author Manuscript
Author Manuscript
Author Manuscript
Author Manuscript

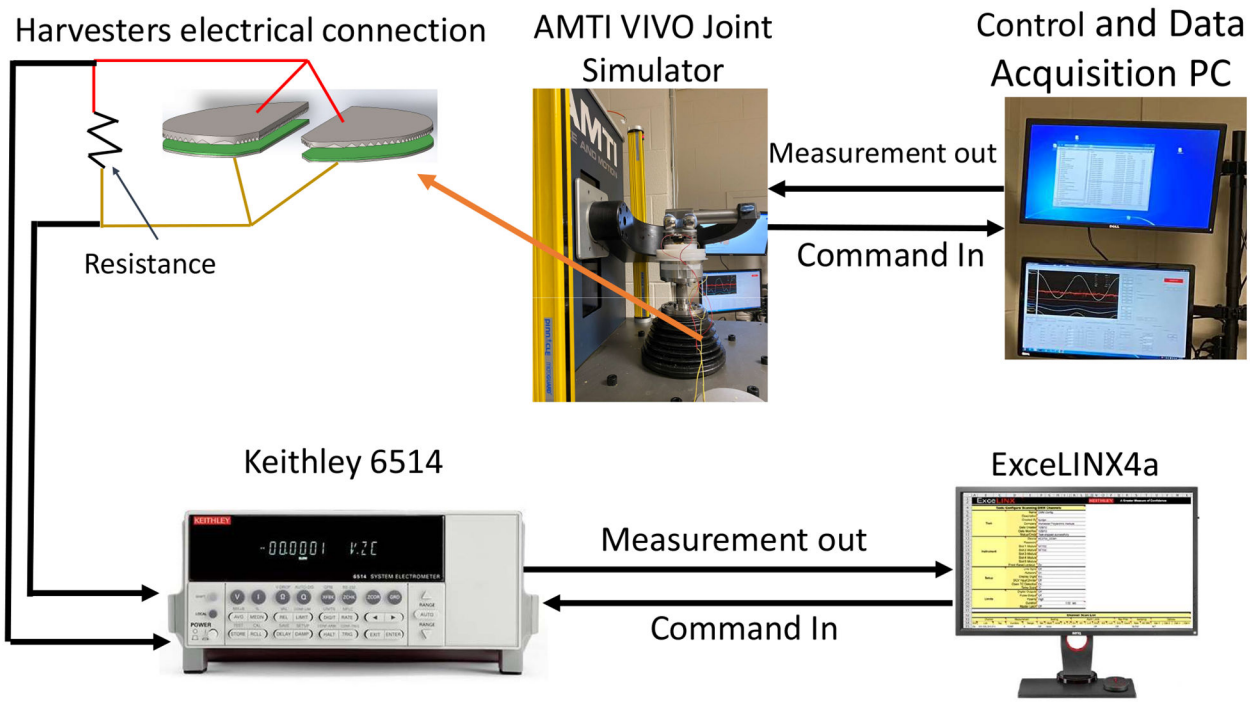

Fig. 4.
A schematic of the experimental setup

Author Manuscript Author Manuscript Author Manuscript Author Manuscript

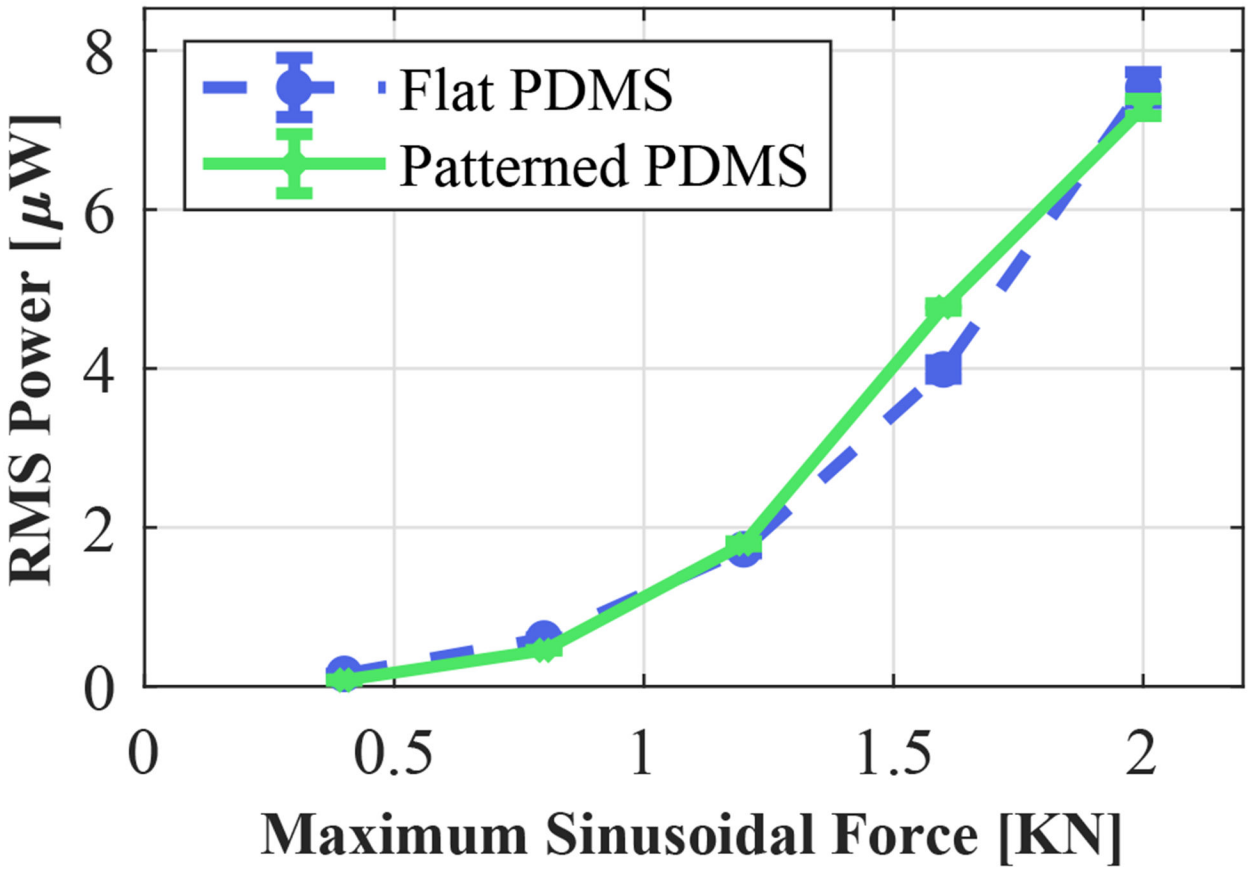

Fig. 5.

RMS power outputs at different maximum sinusoidal loads for the Ti6Al4V package-harvesters assemblies. The minimum of the sinusoidal loads was 50N and the frequency was 1 Hz. Uncertainties on the mean RMS power calculated from 3 sets of 7 cycles of the corresponding voltage signals are shown in error bars.

Author Manuscript Author Manuscript Author Manuscript Author Manuscript

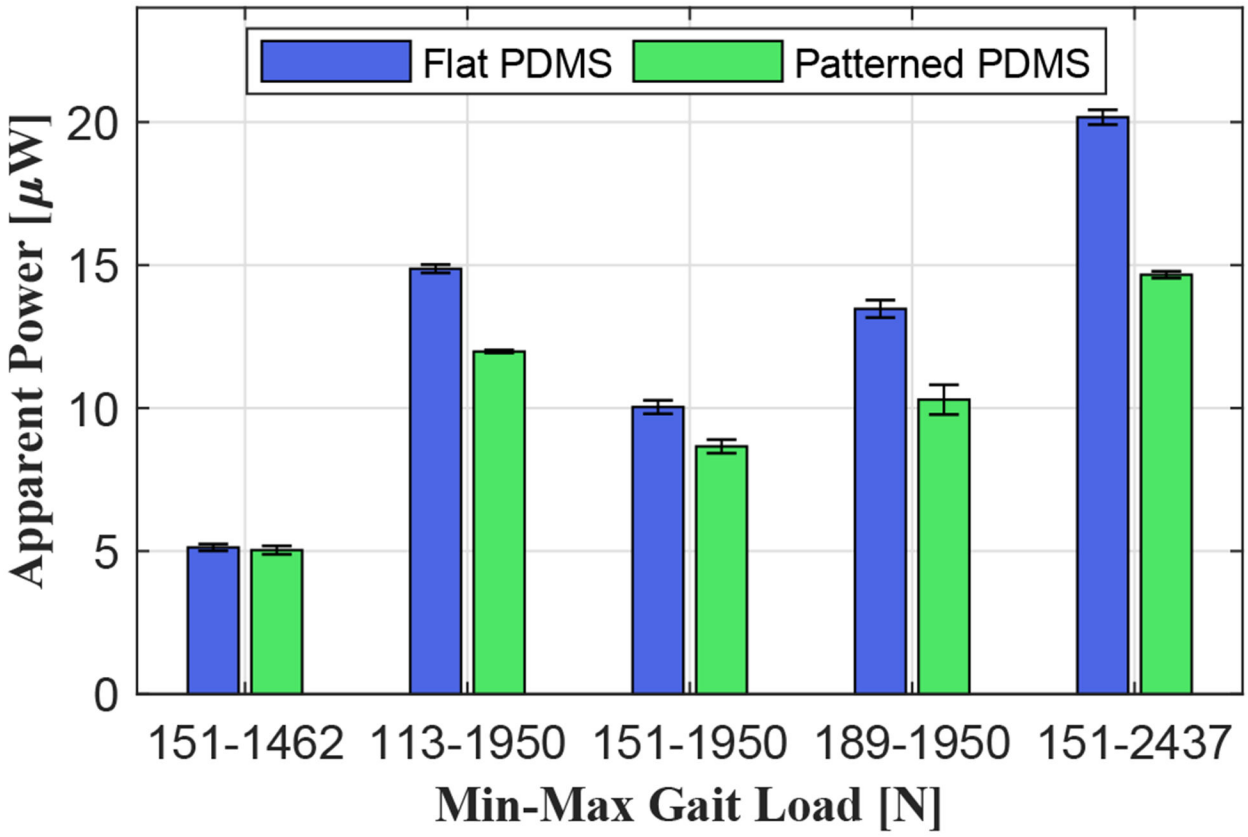

Fig. 6.

Apparent power outputs at various 1-DOF gait cycles (period of the signals = 1 sec) for the Ti6Al4V package-harvesters assemblies. Uncertainties on the mean apparent power calculated from 3 sets of 7 cycles of the corresponding voltage and the current signals are shown in error bars.

Author Manuscript Author Manuscript Author Manuscript Author Manuscript

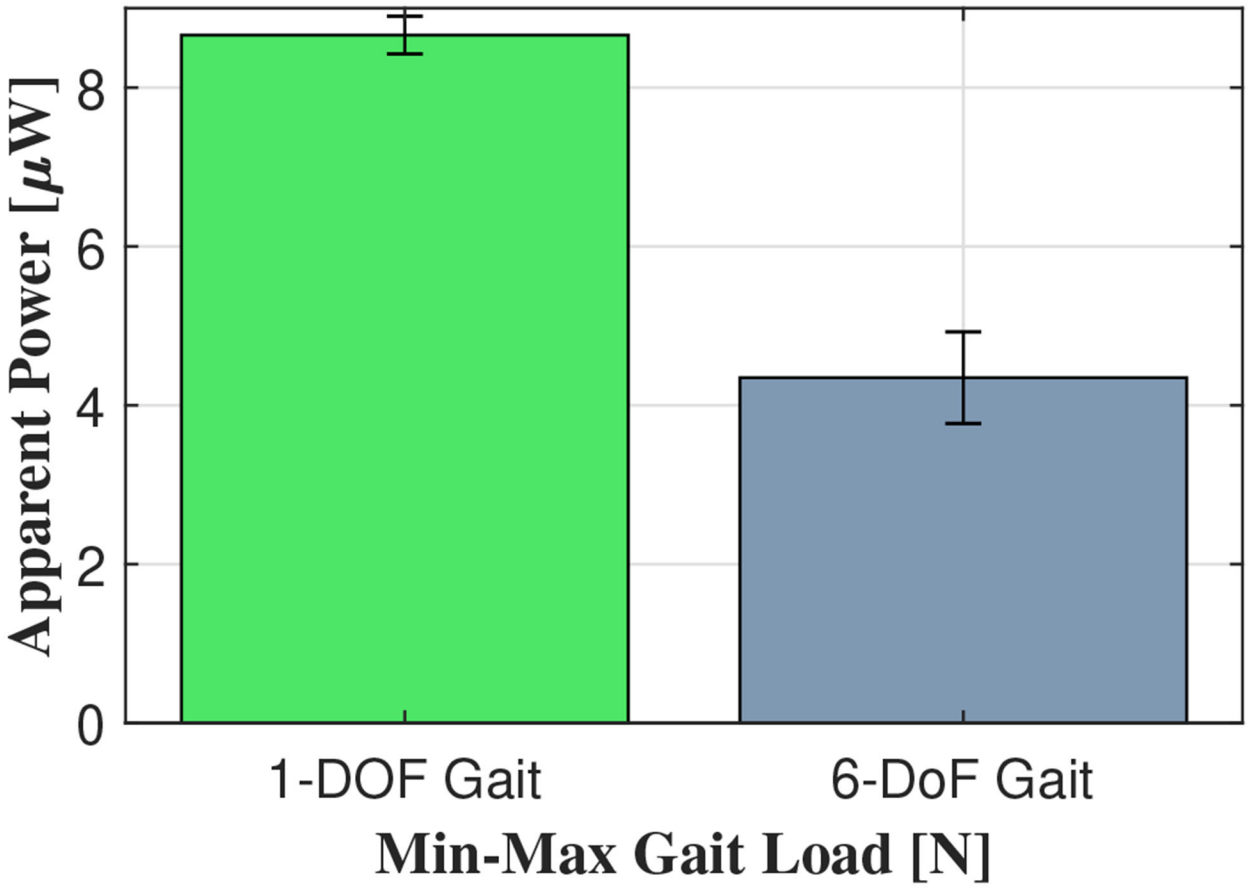

Fig. 7.

Apparent power output from a 1-DOF, and a 6-DoF gait test. Tests were performed on the package-harvester configuration 2 (Patterned PDMS) for the load range of $151 - 1950N$ at a frequency of $1Hz$, and $0.67Hz$ for the 1-DOF and 6-DoF gait, respectively. Uncertainties on the mean apparent power calculated from 3 sets of 7 cycles of the corresponding voltage and the current signals are shown in error bars.

Author Manuscript
Author Manuscript
Author Manuscript
Author Manuscript

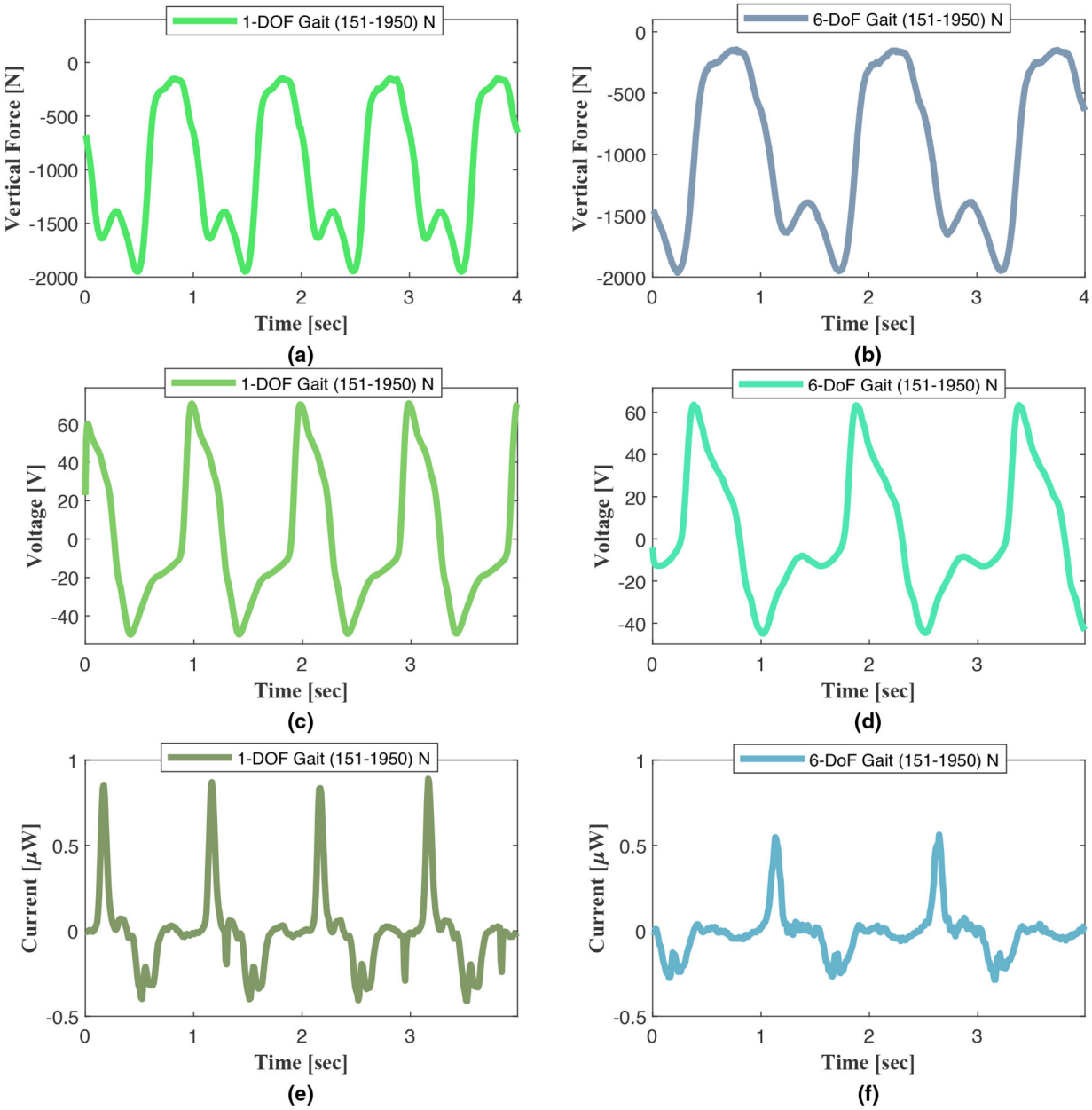

Fig. 8.

(a)–(b) Force response from the knee simulator under 1-DOF, and 6-DoF gait loading of 151–1950*N*. (c)–(d) The corresponding voltage measurement for 1-DOF, and 6-DoF gait loading. (e)–(f) And the respective current measurement for 1-DOF, and 6-DoF gait loading. The input signal frequency was 1*Hz*, and 0.67*Hz* for the 1-DOF and the 6-DoF gait tests, respectively.

Author Manuscript Author Manuscript Author Manuscript Author Manuscript

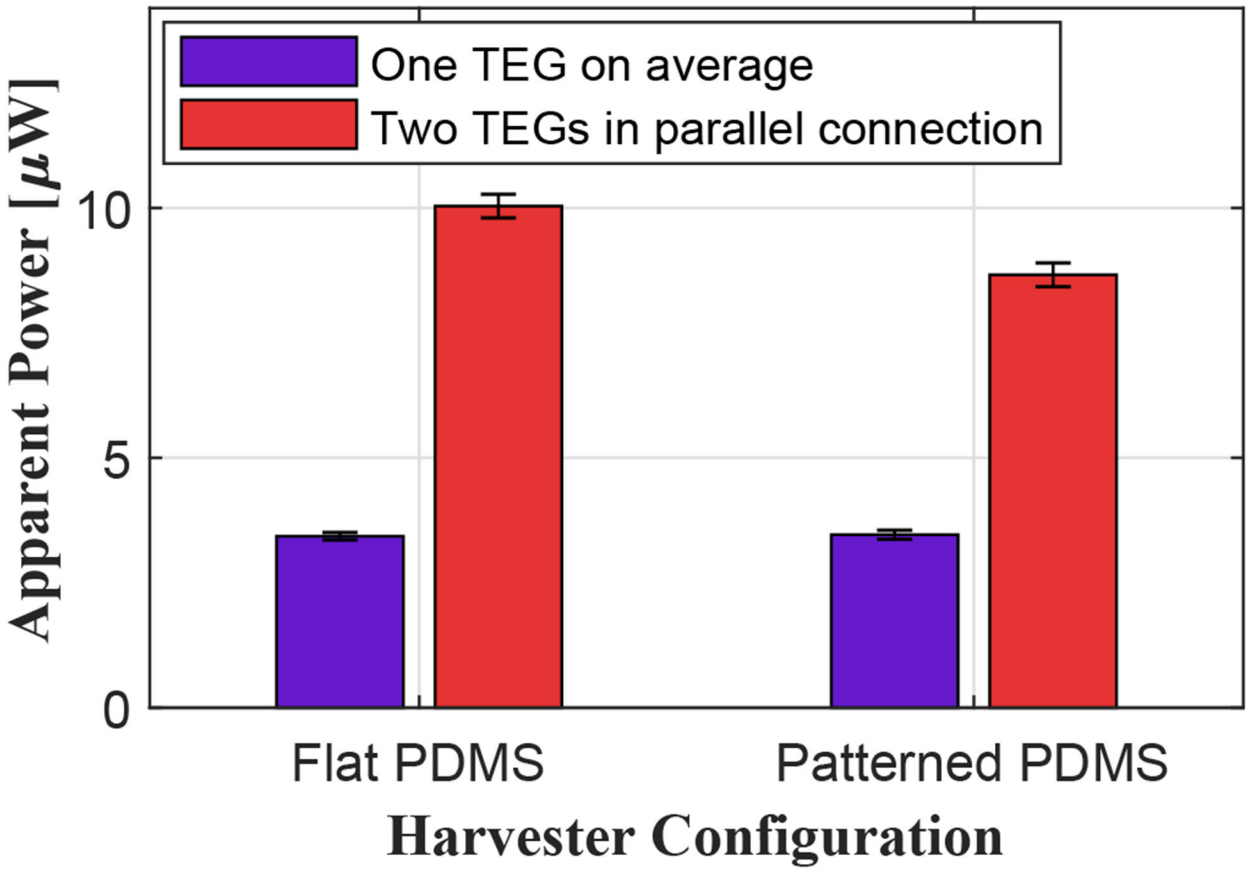

Fig. 9.

Apparent power output comparison between two harvesters and one harvester connection. Each test was conducted under 151 – 1950 N of 1-DOF and 1 Hz frequency. Uncertainties on the mean apparent power calculated from 3 sets of 7 cycles of the corresponding voltage and the current signals are shown in error bars.

Author Manuscript Author Manuscript Author Manuscript Author Manuscript

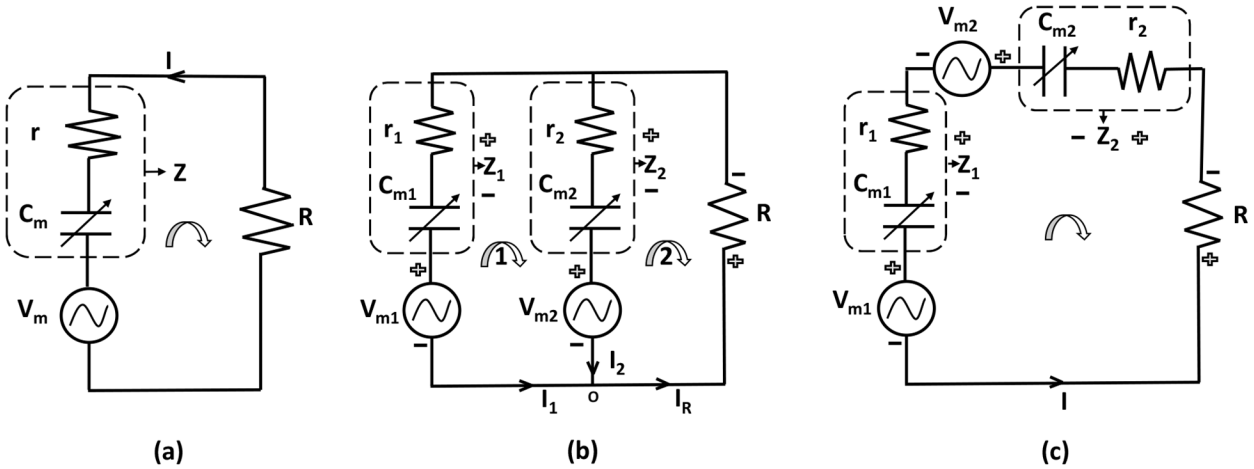

Fig. 10.

Lumped-parameter electrical model for (a) one TEG with an external load resistance, Two TEGs in (b) parallel connection, and (c) series connection with an external load resistance.